ACS APPLIED MATERIALS & INTERFACES

Research Article

www.acsami.org

Comprehensive Study on the Controlled Plasmon-Enhanced Photocatalytic Activity of Hybrid Au/ZnO Systems Mediated by Thermoresponsive Polymer Linkers

Minji Yoon, Ji-Eun Lee, Yu Jin Jang, Ju Won Lim, Adila Rani, and Dong Ha Kim*

Department of Chemistry and Nano Science, Ewha Womans University, Seoul 120-750, South Korea

Supporting Information

ABSTRACT: Hybrid semiconductor/noble metal nanostructures coupled with responsive polymers were used to probe unique plasmon-mediated photocatalytic properties associated with swelling–shrinking transitions in polymer chains triggered by specific external stimuli. Poly(*N*-isopropylacrylamide) (PNIPAM) brushes were anchored on Au films by atom transfer radical polymerization and ZnO nanoparticles were immobilized on the PNIPAM layer to explore controlled photocatalytic activity. The plasmon-enhanced photocatalytic activity was dictated by two critical parameters, that is, grafting density and molecular weight of PNIPAM involved in Au film-PNIPAM-ZnO. The effect of the areal density of PNIPAM chains on the temperature-responsive UV light photocatalytic activities showed mutually antagonistic trends at two different temperatures. The performance at high density was higher above a lower critical solution temperature (LCST), that is, under contracted configuration, while the sample with low density showed higher activity below LCST, that is, extended configuration. Among all the cases explored, the UV light activity was highest for the sample with thin PNIPAM layer and high density above LCST. The visible light activity was induced only for thin PNIPAM layer and high density, and it was higher above LCST. The efficiency of photocatalytic decomposition of phenol pollutant was dramatically enhanced from 10% to 55% upon the increase in temperature under visible light illumination.

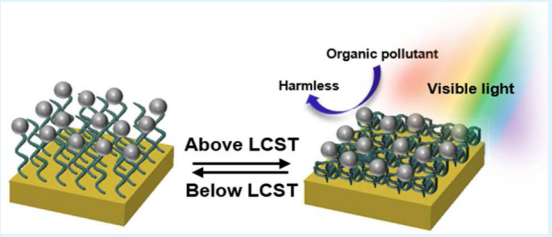

KEYWORDS: *surface plasmon resonance (SPR), photocatalytic activity, Au/ZnO, thermoresponsive polymer, atom transfer radical polymerization (ATRP)*

INTRODUCTION

Semiconductor-based photocatalysis has been considered essential elements in recent energy conversion and fuel production, as well as environmental remediation because of their intrinsic photophysical properties associated with exciton generation. Among the numerous candidates, nanostructured semiconductors, such as zinc oxide (ZnO), have been recognized as promising photocatalytic materials because of its high photosensitivity, nontoxic nature, better exciton ability, and low cost.[1−3] However, the photocatalytic activities of ZnO have been very modest until now, because ZnO has a wide band gap limiting its absorption of UV light, which constitutes only 4% of the total solar spectrum and quick recombination property of charge carriers.[2,4,5] To solve those problems, several strategies such as dye sensitization,[6,7] semiconductor coupling,[8] nonmetal doping[2,9] and plasmonic metal coupling[10−15] have been applied. Among them, coupling effect with noble metal nanostructures such as Au and Ag into ZnO has been proposed as alternative viable approach. Noble metals have unique surface plasmon resonance (SPR) properties resulting from the interaction with light.[11,16] It has been investigated that the SPR induces and improves the efficiency under visible light photocatalytic activity,[16] and the effect is extremely sensitive to the distance between the constituent elements, which is exploited in Plasmon ruler.[17−19] Also noble metals can act as electron trap center where the photon-generated electrons are accumulated.[20]

Stimuli-responsive materials can undergo conformational changes on external environment such as temperature or pH, mechanical force and irradiated light.[21−24] Especially, poly(*N*-isopropylacrylamide) (PNIPAM), one of the representative thermoresponsive polymers, have a wide range of applications including biosensors, drug delivery, and templating hybrid materials.[25−27] In particular, it has been used as distance controller between two materials which interact each other.[28−31] PNIPAM undergoes a reversible phase transition at a lower critical solution temperature (LCST) of ∼32 °C in pure water from a swollen state to a collapsed state upon increasing the temperature because of dissociation of the hydrophobic interaction between NIPAM segments and water.[32] In addition, the polymer chains are swollen and collapsed in a different manner depending on both the grafting density and the molecular weight of PNIPAM.[33,34] With this

Received: May 5, 2015
Accepted: August 14, 2015
Published: August 14, 2015

DOI: 10.1021/acsami.5b03872
ACS Appl. Mater. Interfaces 2015, 7, 21073−21081

complex nature, PNIPAM brushes have been exploited to control the distance between two molecules.[35,36]

The presence of interlayer between noble metal and metal oxide could restrict the coupling of the SPR energy with semiconductor. Also the SPR effect is regulated depending on the thickness of the interlayer and the effect is diminished by thick gap due to limited pathway of energy transfer.[37−39] So, for efficient SP energy transfer caused by excitation of noble metals, it is a crucial factor to define the optimum distance. However, any systematic investigations into the effect of diverse parameters involved in the temperature-responsive PNIPAM chains on the UV and visible light active photocatalysis in hybrid metal/semiconductor systems are lacking.

Considering this critical issue yet to be explored, in this paper, we developed hybrid ZnO/Au films modulated by PNIPAM brushes having different molecular weight and density, and systematically demonstrated the effect of configuration-controlled PNIPAM interlayer in the plasmon-enhanced photocatalysis. The proposed schematic diagram for the photocatalysis depending on temperature in our system is depicted in Figure 1. First, PNIPAM brushes were anchored on

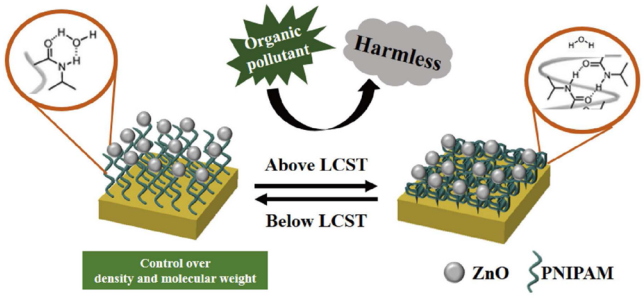

Figure 1. Schematic illustration of the hybrid Au film and ZnO NPs system coupled with PNIPAM chains with controlled density and molecular weight designed for the comprehensive investigation of plasmon-coupling-based visible light driven photocatalytic activity. The photocatalytic activity can be observed as phenol pollutant decomposition.

the Au film by atom transfer radical polymerization (ATRP) and the molecular weight and density of the polymer layer were controlled by changing the reaction conditions.[40−43] Next, synthesized ZnO nanoparticles (NPs) were immobilized on PNIPAM layer for controlled photocatalytic activity. On the basis of the Au film-PNIPAM-ZnO hybrid structure, plasmonic coupling effect is controlled by changing the gap between Au films and ZnO NPs, that is, by changing the temperature with respect to the LCST. We systematically demonstrated photocatalytic activities of the hybrid nanostructure with different molecular weight and density of polymer under UV and visible light.

MATERIALS AND METHODS

Materials. CuBr, disulfide initiator ([S−$(CH_2)_{11}$−OCOC−$(CH_3)_2$Br], *N*-isopropylacrylamide (NIPAM, 97%), $HAuCl_4$, sodium azide, 2-proprgylamine, copper(II) sulfate, L-ascorbic acid sodium salt, and PMDETA were purchased from Sigma-Aldrich for preparing Au film-PNIPAM hybrid film. Zinc nitrate hexahydrate ($Zn(NO_3)_2$ $6H_2O$), ammonia hydroxide (28 wt % NH_3 in water.) and starch powders were purchased from Sigma-Aldrich for preparing ZnO particles. *p*-nitrophenol (PNP) was purchased from Sigma-Aldrich.

Synthesis of Au Film-Initiator. A 50 nm thick Au layer on silicon substrate with 2 nm thick Cr adhesion layer was used for the incorporation of PNIPAM layer. Bare Au film was immersed into a 10 mL disulfide initiator solution (6 μL, 1.0 mM) in ethanol for 1 and 24 h, repectively to control density of PNIPAM. Then, the Au film-initiator substrate was collected and washed with ethanol and deionized water.

Synthesis of Au Film-PNIPAM. The thermoresponsive PNIPAM layer was fabricated by reacting bromo end group groups on the Au film-initiator with NIPAM monomers by ATRP method. A round-bottom Schlenk flask was filled with CuBr (12.5 mg, 0.085 mmol), NIPAM (0.905 g, 8 mmol), and Au film-initiator substrate with −Br groups degassed by three freeze−pump−thaw cycles in N_2 atmosphere. Wherein, a mixture of H_2O (15.2 mL) and methanol (2 mL) was injected into the flask through a syringe. The reaction was performed for 1 h at room temperature and terminated by opening the system to air. Finally the Au film-PNIPAM substrate was rinsed with water.

Synthesis of ZnO Nanoparticles. Synthesis of ZnO NPs were performed according to a previous reported method.[44] Five grams of soluble starch was dissolved in 150 mL of boiling deionized water. Then, 0.01 mol of $Zn(NO_3)_2{\cdot}6H_2O$ was added to the resulting clear starch solution, and the mixture was stirred at 85 °C for 5 min. The pH of the mixture solution was then adjusted by 5 mL, and addition of ammonium hydroxide and opaque solution was obtained. The solution was stirred for an additional 30 min at 85 °C, and the resulting precipitate was centrifuged, washed with deionized water, and dried at 50 °C.

Immobilization of ZnO Nanoparticles on Au Film−PNIPAM Substrate. We prepared amine-terminated PNIPAM for facile decoration of ZnO NPs. First, Au film-PNIPAM substrate was immobilized in sodium azide (65 mg, 1 mmol) and DMF (10 mL) solution for 1 h at room temperature for conversion of bromo-end groups of PINPAM to azide functional group. Second, to introduce amine functionality, copper[45] sulfate (0.24 mg, 0.15 mmol), and L-ascorbic acid sodium salt (6.6 mg, 0.0375 mmol) were added into a Schlenk flask. The system was degassed by three freeze−pump−thaw cycles in N_2 atmosphere for ambient condition. Wherein, mixtures of water (12.5 mL), ethanol (12.5 mL), and 2-propargylamie were injected into the flask through a syringe. After 24 h at 25 °C amine-terminated PNIPAM film was obtained. Finally, ZnO NPs were adsorbed on top of the PNIPAM chains through electrostatic and physical interaction by immersing the functionalized substrates in the ZnO NP solution for 8 h.

Instruments and Measurements. Surface morphologies and thickness of the hybrid film were investigated with an atomic force microscope (AFM) in tapping mode (Digital Instruments Dimension 3100 scanning force microscope) and scanning electron microscopy (SEM; JEOL JSM6700-F). ATR-FT-IR measurements were carried out using an FTIR spectrometer (Varian, Scimitar series). UV−vis absorbance was measured using a Sinco S-4100 spectrometer. The incident photon-to-current conversion efficiency (IPCE) was measured using a K3100 HS technology Inc. measurement system with bias light.

Photocatalytic Measurements. The photocatalytic degradation of the organic compound on Au film−PNIPAM−ZnO hybrid film was tested under both UV (λ = 254 nm) and visible light irradiation. For photocatalytic measurements, the hybrid film was immersed in 10 ppm *p*-nitrophenol (PNP) solution and the solution was kept under stirring. A container containing the PNP solution was dipped in water bath and the temperature was controlled by hot plate. The photocatalytic measurements was performed at both 28 °C (Below LCST) and 35 °C (Above LCST). The sample was irradiated using Xe lamp (Newport Co. Ltd., Model 66984) which can illuminate 200−2500 nm light equipped with a 420 nm cutoff filter (long pass filter) at a power of 300 W as a visible light source. The decrease in absorbance of a certain characteristic peak of PNP was measured at regular intervals using UV−vis spectroscopy (Varian Cary5000 UV−vis-NIR spectrophotometer).

FDTD Simulation. A commercial software of three-dimensional Full WAVE FDTD software purchased from Synopsys, Inc., is used to simulate the near-field distribution of the ZnO NPs on Au film-

DOI: 10.1021/acsami.5b03872
ACS Appl. Mater. Interfaces 2015, 7, 21073−21081

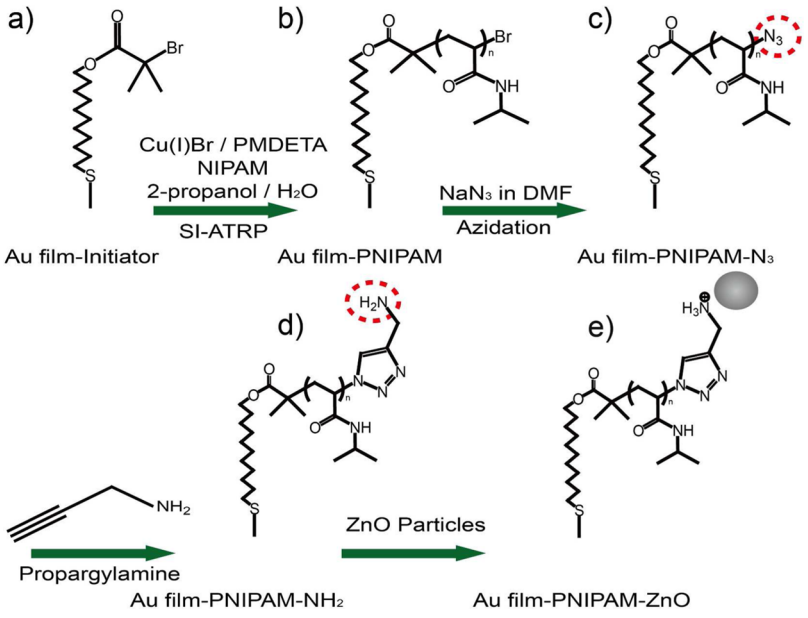

Figure 2. Schematic illustration of the preparation of Au film-PNIPAM-ZnO. (a) Initiator for initiating polymerization was decorated on the Au film surface. (b) PNIPAM chains were polymerized through ATRP. (c) End group of PNIPAM chains (−Br) was changed into $-N_3$ with azidation reaction. (d) The end group of PNIPAM chains ($-N_3$) was changed into $-NH_2$ group to obtain positive charged ending. (e) ZnO particles were decorated on the PNIPAM chains through chemical and physical interactions.

PNIPAM. For the calculation, a plane wave source and DFT frequency analysis was used. The simulation domain for z direction was used by a perfectly matched layer (PML) to absorb all the field propagating to the outer, while x and y directions was periodic boundary conditions. In the mesh domain, 5 nm of uniform grid size is set for all directions. The electric field density at 500 nm wavelength is calculated to confirm the field distribution by the hybrid structure.

RESULTS AND DISCUSSION

The entire stepwise procedure to obtain Au−PNIPAM−ZnO film is depicted in the Figure 2. PNIPAM linkers were synthesized by ATRP and the end group of the PNIPAM was modified for easy decoration of ZnO NPs. (Some surface of ZnO are terminated with O^{2-} anions, resulting in negative surface).[46] Amine modified PNIPAM and ZnO NPs are readily bound each other by specific interaction.

The FT-IR spectra of a bare Au film and the one anchored with PNIPAM are shown in Figure 3. In the FT-IR spectrum, the absorption bands detected at 1650, 1370, and 2970 cm^{-1} are characteristic of the −C═O stretching, the mixed vibration of −C−H and −N−H, and antisymmetric deformation $-CH(CH_3)_2$ groups of the grafted PNIPAM, respectively. These results evidence the formation of PNIPAM layer. The surface morphology of the sample for each step of the entire fabrication procedure was investigated by AFM and SEM images as shown in Figure 4. Figure 4a and b illustrate the AFM

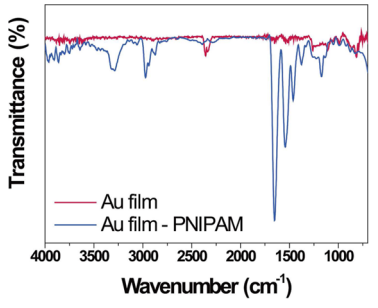

Figure 3. FR-IR spectrum of Au film-PNIPAM. The absorption bands detected at 1650, 1370, and 2970 cm^{-1} are characteristic of the −C═O stretching, the mixed vibration of −C−H and −NH, and antisymmetric deformation $-CH(CH_3)_2$ groups of the grafted PNIPAM, respectively.

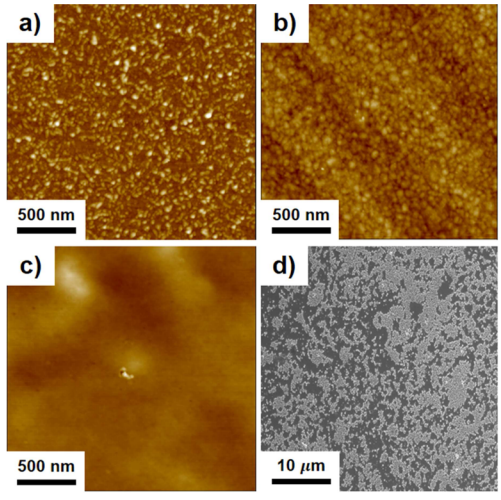

Figure 4. AFM images of (a) bare Au film, (b) after initiator immersion (Au film−initiator), (c) after polymerization of PNIPAM brushes by ATRP method (Au film−initiator−PNIPAM),and (d) after decorating ZnO particles (Au film−initiator−PNIPAM−ZnO).

images of a bare Au film and an identical substrate after functionalization with disulfide initiator by ligand exchange reaction, respectively. No significant difference was found between the two morphologies. In comparison, the surface after PNIPAM synthesis shows a smooth morphology because the entire surface of the film was fully covered with polymer chains as shown in Figure 4c. The ZnO NPs loaded on the surface of

DOI: 10.1021/acsami.5b03872
ACS Appl. Mater. Interfaces 2015, 7, 21073−21081

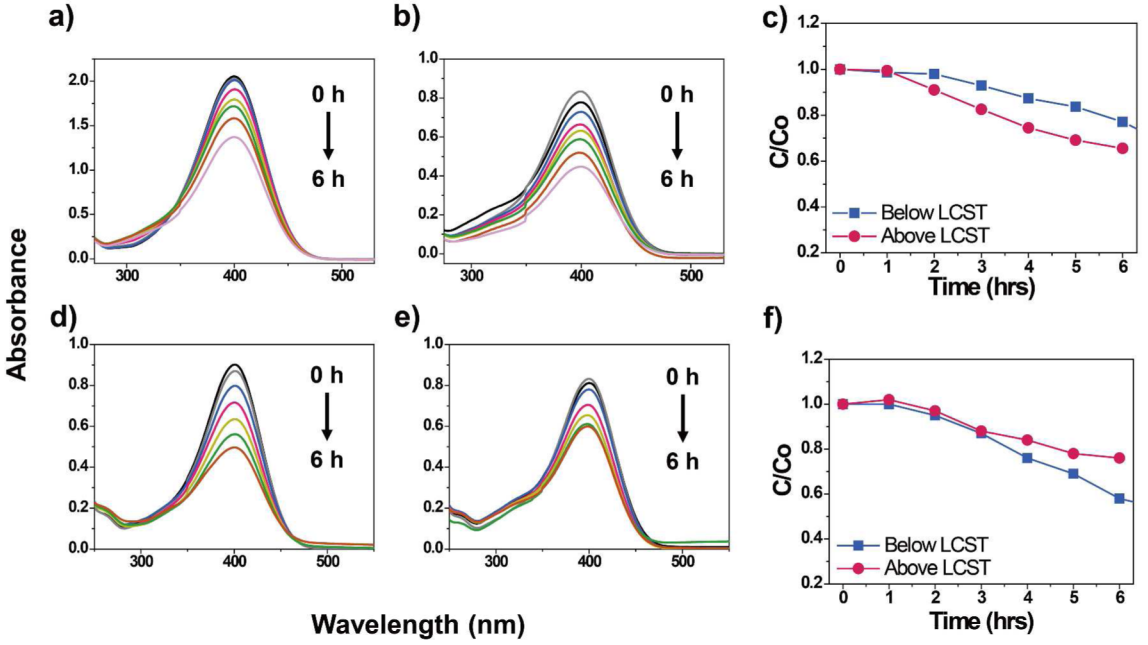

Figure 5. Photocatalytic degradation of PNP using Au film−PNIPAM (1 h)−ZnO hybrid nanostructure with thick PNIPAM film and two different PNIPAM density prepared at 1 h polymerization time under UV−vis irradiation. Absorption spectra with 1 h intervals (a, b) and decolorization efficiency versus time curves (c) obtained from the samples with high PNIPAM density treated with initiator solution during 1 h. Absorption spectra with 1 h intervals (d, e) and decolorization efficiency versus time curves (f) obtained from the samples with low PNIPAM density treated with initiator solution during 24 h.

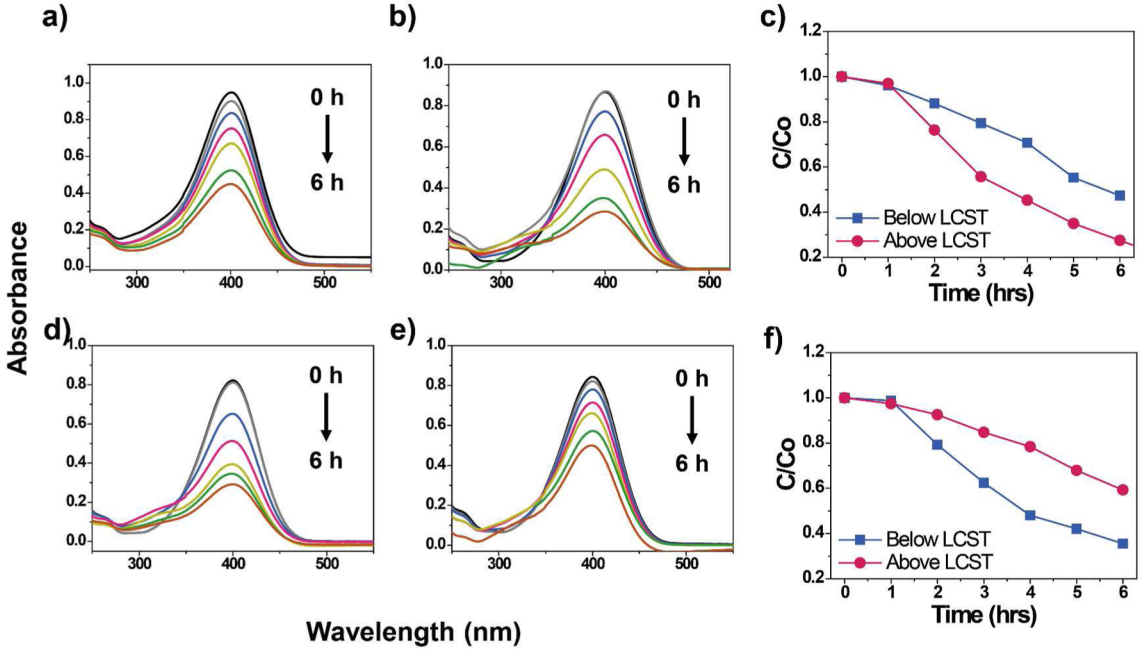

Figure 6. Photocatalytic degradation of PNP using Au film−PNIPAM−ZnO hybrid nanostructure with thin PNIPAM film and two different PNIPAM density prepared at 30 min polymerization time under UV−vis irradiation. Absorption spectra with 1 h intervals (a, b) and decolorization efficiency versus time curves (c) obtained from the samples with high PNIPAM density treated with initiator solution during 1 h. Absorption spectra with 1 h intervals (d, e) and decolorization efficiency versus time curves (f) obtained from the samples with low PNIPAM density treated with initiator solution during 24 h.

Au film-PNIPAM exhibits uniform dispersion as shown in Figure 4(d)

We systematically demonstrate the photocatalytic activity of the system by controlling two critical parameters related with the stimuli-sensitive polymer layer. Concretely, the molecular weight and density of the PNIPAM were controlled by handling polymerization time and disulfide initiator dipping time, respectively. Controlling the molecular weight results in the change in the thickness of PNIPAM layer. The AFM topography images of PNIPAM layer with different polymerization time are listed in Figure S1. Four types of PNIPAM samples were prepared with different synthesis time (60, 45, 30,

DOI: 10.1021/acsami.5b03872
ACS Appl. Mater. Interfaces 2015, 7, 21073−21081

and 15 min) and each sample shows 40, 20, 15, and 10 nm thickness, respectively, according to the cross-sectional height profiles obtained from the AFM images. To assess the density of PNIPAM chains, citrate-capped AuNPs having negative surface charge were immobilized onto the amine-terminated PNIPAM layer driven by electrostatic interaction, and the surface morphology was investigated by SEM images. Distinctly different density of Au NPs, that is, different density of PNIPAM chains, was confirmed from different samples as shown in Figure S2. To compare the photocatalytic activity of the samples with different types of PNIPAM layer, it is necessary that the same amount of ZnO NPs be introduced in the nanostructures. It was found that almost the same amount of ZnO NPs were immobilized onto the amine-terminated PNIPAM layer with different density when the films were treated with ZnO NP solution for 8 h (Figure S3). Thus, we employed this experimental protocol (8 h dipping in ZnO NP solution) for objective comparison from different samples.

The absorption spectra of ZnO nanoparticles, Au film, and Au film-PNIPAM were measured in Figure S4. ZnO NPs exhibit strong absorbance in the range of UV light in contrast to Au film which responds to visible light. Consequently, Au film−PNIPAM−ZnO hybrid film shows both UV and visible light absorption because of the presence of ZnO and Au film. It was reported that the enhanced optical absorbance at visible region results in enhanced photocatalysis,[47] implying that the model system used in this study can exhibit enhanced visible light photocatalytic performance.

The photocatalytic activity of hybrid thermoresponsive nanostructure under UV light illumination was evaluated in terms of the degradation of harmful organic compound PNP. The decrease in the absorbance of the characteristic peak of PNP at 400 nm was monitored for each of the samples as displayed in Figures 5 and 6. To confirm the different activity depending on molecular weight and density of PNIPAM, four different samples were prepared by controlling the thickness and density of the PINIPAM. Density was controlled by applying different initiator dipping time of 1 and 24 h, and the thickness was controlled by adjusting PNIPAM polymerization time of 30 min and 1 h. The hybrid film prepared from two conditions, that is, Au substrates immersed in initiator solution during 1 and 24 h, showed strikingly different behavior with changing the temperature. However, it was observed that PNP degradation rate is almost the same with changing the temperature in the case of the sample prepared from 3 h immersion in initiator solution (Figure S5b). Eventually, four different samples were prepared for systematic comparison, that is, Au film-initiator (24 h)−PNIPAM (1 h), Au film−initiator (24 h)−PNIPAM (30 min), Au film−initiator (1 h)−PNIPAM (1 h), and Au film−initiator (1 h)−PNIPAM (30 min).

Figure 5 illustrates the photocatalytic activity of the hybrid film prepared from 1 h polymerization time with different density. Figure 5a−c are the results from the sample of 24 h immersion in initiator solution, and Figure 5d−f are the results from the one of 1 h immersion in initiator solution. It was found that Au film−PNIPAM−ZnO hybrid structure with denser PNIPAM chains (24 h immersion in initiator solution) showed better photocatalytic enhancement (from 35% to 43%) when the temperature was increased above the LCST. This observation is interpreted as the result of reduced distance between the Au and ZnO driven by collapsed polymer configuration.

However, directly opposed results were obtained for the Au film−PNIPAM−ZnO hybrid structure with less dense PNIPAM chains (1 h immersion in initiator solution) as shown in Figure 5d−f. It is observed that the overall photocatalytic activity was better below LCST and the degree of degradation was decreased from 49% to 28% with temperature increasing. This result can be explained in terms of the effect of large space between each neighboring polymer chain.[48] The polymers form standing brushes in packed configuration in the case of high density environment. Reversely, each polymer is in the nonoverlapping mushroom regime when the space between each polymer is large. So the gap between Au film and ZnO becomes smaller at low temperature. In this way, the gap between Au film and ZnO becomes relatively larger at high temperature compare to low temperature. Accordingly the effect of the electron transfer is diminished as the temperature increases. The above results were summarized and compared in Figure 5c and f, wherein one can observe different photocatalytic activity depending on PNIPAM density as the temperature increases. To the best of our knowledge, this work is the first report on the effect of multiple experimental parameters on the photocatalytic activity of hybrid metal−semiconductor system mediated by responsive polymers. However, it is noted that the overall large gap between Au film and ZnO led to negative effect on the photocatalytic effect.

On the basis of the above studies, next, different hybrid structures with much thinner PNIPAM layer was prepared in order to induce plasmon energy transfer. The thickness of the hybrid film was measured to be ∼15 nm as shown in Figure S1, which can be controlled by PNIPAM polymerization time. The photocatalytic activity based on this hybrid film was investigated and summarized in Figure 6. When the polymer density was high, photocatalytic activity was significantly improved from 52% to 72% as the temperature increased. In contrast, the photocatalytic activity was diminished from 64% to 40% in the case of low PNIPAM density. Similar to the observation made for the samples with thick PNIPAM layer, mutually opposed photocatalytic activity was obtained for the samples with high and low density PNIPAM as the temperature increases. It is found that significantly enhanced photocatalytic activity was observed compared to thick film because of smaller gap between Au film and ZnO NPs which causes electron transfer. Upon illumination of UV light, electrons of valence band (VB) of ZnO are excited to the conduction band (CB), leaving holes in the VB of the ZnO particles.[10] Then the excited electrons are transferred to Au and hence the immediate recombination is suppressed. This mechanism promotes the separation of electrons and holes, and the enhancement of photocatalytic activity can be obtained. It is noted that this mechanism applies only in case the Au and ZnO intact each other, which was reflected in the obtained experimental results.

To demonstrate the plasmonic effect on the enhanced photocatalysis as a function of the interdistance, photocatalytic activity under visible light illumination was investigated (Figure 7). It was reported that plasmonic effect could induce visible light photocatalytic activity of ZnO.[3,49] It is noted that visible-light-driven decomposition of PNP was not observed for the hybrid film having relatively high molecular weight and low density of PNIPAM. This result suggests that the PNIPAM layer should be thin enough to induce visible light activity. In previous studies, it was reported that the plasmon energy transfer could work most effectively when the thickness of

DOI: 10.1021/acsami.5b03872
ACS Appl. Mater. Interfaces 2015, 7, 21073−21081

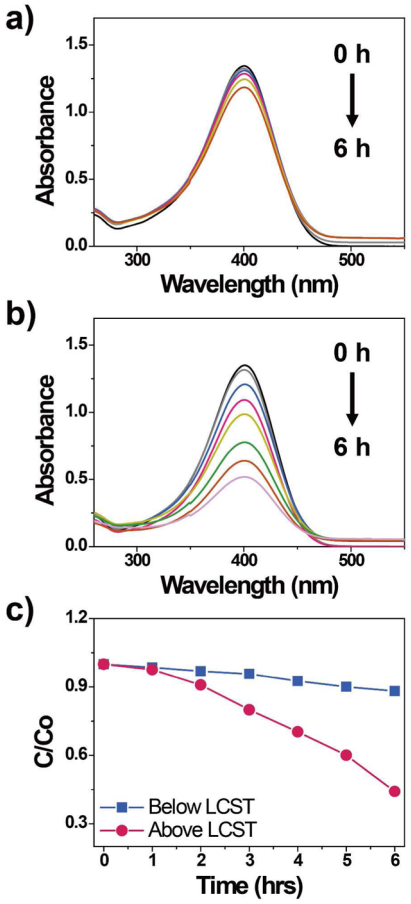

Figure 7. Photocatalytic degradation of PNP using Au film−PNIPAM (15 min)−ZnO hybrid nanostructure with even thinner PNIPAM film and higher PNIPAM density prepared at 15 min polymerization time under visible irradiation. Absorption spectra with 1 h intervals (a, b) and decolorization efficiency versus time curves in panel c.

space layer between Au and TiO_2 is about 5−10 nm.[39,50] Thus, a model system with thinnest PNIPAM having 10 nm thickness prepared from 15 min polymerization time was used to investigate visible light photocatalytic activity. Also hybrid films having high density was selected because thin PNIPAM of low density could not be synthesized uniformly. In Figure 7a, it was observed that the hybrid film with 10 nm gap between the Au and ZnO showed negligible photocatalytic ability at lower temperature. In contrast, the hybrid film exhibits a remarkably higher visible light photocatalytic activity at higher temperature, due to smaller gap between Au film and ZnO NPs as shown in Figure 7b. This result evidence that the ZnO NPs and Au films are in close contact each other when PNIPAM chains are collapsed. This situation can allow for facile plasmon energy transfer from Au film to ZnO. Thus, tremendous increase in photocatalytic efficiency from 10% to 55% was observed with increasing the temperature as shown in Figure 7c.

The photocatalytic mechanism under irradiation with visible light is similar to electron injection from metal film to the semiconductor. Electron transfer mechanism between plasmonic structure and semiconductor was already investigated in several researches.[51,52] Enhanced photocatalytic activity of ZnO−Au system can be explained by facilitated exciton separation via two mechanism, that is, (i) via the transfer of CB electron in ZnO to Fermi level of Au under UV light excitation, and (ii) via SP-induced energetic hot electron transfer from Au to the CB of ZnO under visible light excitation (Figure S7). The work function values of ZnO and Au are reported as 5.2 and 5.0 eV, respectively. Therefore, the hot electrons generated by visible light induced surface plasmon excitation can transfer from the Au to the ZnO level, until it reaches the equilibrium state. Upon irradiation with visible light, the hot electrons via SP excitation are injected to the CB of ZnO, leaving holes on the metal surface. Then the injected electrons in CB of ZnO reacts with oxygen dissolved in water to produce superoxide radical anion, which can react with water molecule to give hydroxyl radicals. The superoxide radical anion and hydroxyl radicals react with phenol pollutant. Upon excitation by incident light, the surface plasmon polariton (SPP) of Au film results in an enhanced overall confined electrical field close to the Au film surface as well as giant field enhancements near the surface of Au film up to 300 nm.[53] Then, plasmon resonance energy transfer from Au film to ZnO occurs through coupling of the SPP of Au film with the band gap energy of ZnO.[37] Consequently, hot electron transfer was tuned by controlling the distance between Au film and ZnO.[54] Furthermore, the enhanced field could prevent electron and hole from recombination because more electrons and holes are generated and transferred swiftly.[55,56] It was found that the enhanced SPR effect caused by noble metal affected ZnO more effectively in the case of 10 nm gap.[18,39] Conclusively, decreased gap resulting from collapsed polymer configuration led facile plasmon energy transfer from Au film to ZnO as the temperature was increased.

In order to support the wavelength-dependent photocatalysis, incident photon-to-current efficiency (IPCE) measurement was performed in Figure 8. IPCE spectrum was

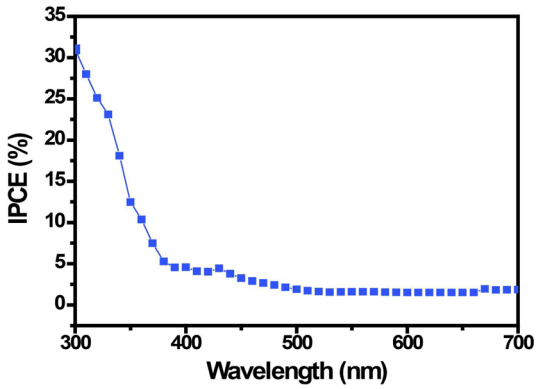

Figure 8. Incident photon-to-current conversion efficiency (IPCE) curves of Au film−PNIPAM−ZnO hybrid film below the LCST (28 °C) under visible light (300−700 nm).

analogous to an absorption spectrum of Au film−PNIPAM−ZnO as shown in Figure S4. Additionally, the FDTD simulation analysis was performed to demonstrate the distribution and influence of the plasmon near field in Figure S7. The field distribution was calculated using the Au film−PNIPAM (10 nm)−ZnO hybrid structure. From the literature[53] and simulation data, it is confirmed that ZnO NPs are located within the enhanced SP field, indicating that plasmon-induced visible light active photocatalysis can occur in the current system.

The stability of the hybrid photocatalyst is of great importance if the catalyst is to be substantially applicable. The stability of PNIPAM for 3 cycles depending on

DOI: 10.1021/acsami.5b03872
ACS Appl. Mater. Interfaces 2015, 7, 21073−21081

temperature was investigated in Figure S8, where it was confirmed that the as-prepared hybrid photocatalysts could be used repeatedly. We also proved the stability of PNP solution under UV−vis illumination. It was reported that the decomposition of PNP solution without suitable catalyst is difficult and this was verified in our control experiment (see dotted curve in Figure S9). Also, a control experiment with Au/ZnO film without PNIPAM was included in Figure S9. It was found that the photocatalytic activity was not affected by the temperature change without thermoresponsive polymer (PNIPAM), which means that PNIPAM plays a critical role in temperature-sensitive photocatlaysis. Finally, the overall photocatalytic performances at different conditions explored in this study were summarized and compared in Figure 9.

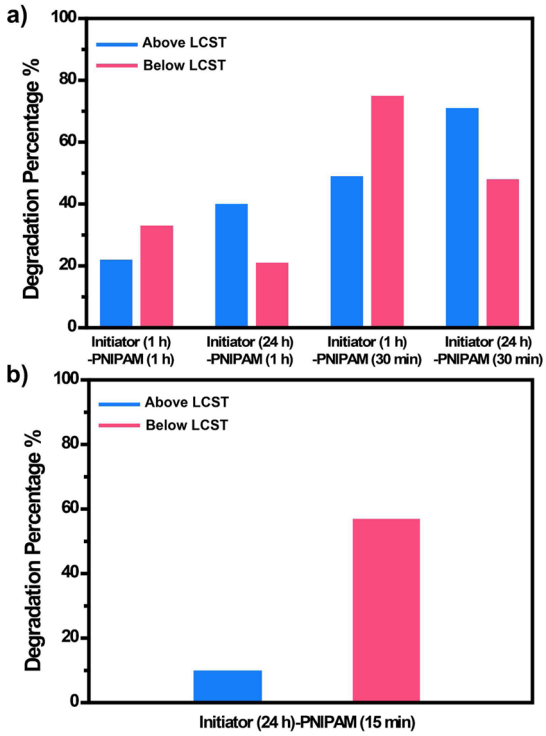

Figure 9. Photocatalytic degradation of PNP at different conditions under (a) UV light and (b) visible light. The experiment was performed at two different temperature, 28 °C (below LCST; blue) and 35 °C (above LCST; red), respectively.

In this work, hybrid ZnO/Au films modulated by PNIPAM brushes having different molecular weight and density were developed for the first time. On the basis of this responsive metal−semiconductor hybrid system, plasmon-enhanced photocatalysis was systematically demonstrated in terms of the configuration-controlled PNIPAM interlayer as a step forward.

CONCLUSION

In conclusion, we developed an effective and useful plasmon-enhanced photocatalytic system based on hybrid metal and semiconductor connected with responsive polymer linkers and UV- or visible light active photocatalysis was demonstrated in a comprehensive and systematic manner. Au film and ZnO NPs were separated by PNIPAM layers with different configurations, that is, controlled density and thickness. Polymer chain density and thickness were regulated by adjusting initiator dipping time and polymerization time, respectively.

When the polymer density was high, the photocatalytic activity was significantly improved from 52% to 72% as the temperature increased. In contrast, the photocatalytic activity was diminished from 64% to 40% in the case of low PNIPAM density. Overall, the system with low molecular weight polymer chains showed better activity under UV-light in terms of the degradation of PNP than high molecular weight polymer.

Photocatalytic activity under visible light was only observed when the distance between Au film and ZnO NPs was very short. Plasmon energy transfer is very sensitive to the gap between Au film and ZnO and play a very crucial role in visible light photocatalytic activity. It was observed that visible light photocatalytic activity increased from 10% to 55% as the temperature increased.

Several experimental demonstrations about temperature-dependent photocatalytic activity have been reported, but the previous works were limited to obtain stimuli-dependent performance phenomenologically. In this study, for the first time we demonstrated that the plasmonic effect in stimuli-sensitive metal−semiconductor system is highly correlated with the configuration involved in the constituent components in dictating the resultant photocatalytic activity. The overall observation and conclusion drawn in this article can be utilized in the design of hybrid photocatalytic system applicable in complex environments or media and considered as generalized protocol to be expanded to other types of materials or devices in the fields of solar-fuel generation, catalysis, sensing, light emission, etc.

ASSOCIATED CONTENT

Supporting Information

The Supporting Information is available free of charge on the ACS Publications website at DOI: 10.1021/acsami.5b03872.

AFM and SEM images of the hybrid films fabricated in different experimental parameters (PDF)

AUTHOR INFORMATION

Corresponding Author

*Tel.: +82-2-3277-4517. Fax: +82-2-3277-4546. E-mail: dhkim@ewha.ac.kr.

Notes

The authors declare no competing financial interest.

ACKNOWLEDGMENTS

This work was supported by National Research Foundation of Korea Grant funded by the Korean Government (2014R1A2A1A09005656; 2014043187), the Commercializations Promotion Agency (COMPA) for R&D Outcomes funded by the Ministry of Science, ICT, and Future Planning (MISP), and the National Research Council of Science and Technology through the Degree & Research Center program (DRC-14-3-KBSI).

REFERENCES

(1) Jang, Y. H.; Kochuveedu, S. T.; Cha, M.-A.; Jang, Y. J.; Lee, J. Y.; Lee, J.; Lee, J.; Kim, J.; Ryu, D. Y.; Kim, D. H. Synthesis and Photocatalytic Properties of Hierarchical Metal Nanoparticles/ZnO Thin Films Hetero Nanostructures Assisted by Diblock Copolymer Inverse Micellar Nanotemplates. *J. Colloid Interface Sci.* **2010**, *345*, 125−130.

(2) Kochuveedu, S. T.; Jang, Y. H.; Jang, Y. J.; Kim, D. H. Visible Light Active Photocatalysis on Block Copolymer Induced Strings of

DOI: 10.1021/acsami.5b03872
ACS Appl. Mater. Interfaces 2015, 7, 21073−21081

ZnO Nanoparticles Doped with Carbon. *J. Mater. Chem. A* **2013**, *1*, 898−905.
(3) Tian, C.; Zhang, Q.; Wu, A.; Jiang, M.; Liang, Z.; Jiang, B.; Fu, H. Cost-Effective Large-Scale Synthesis of ZnO Photocatalyst with Excellent Performance for Dye Photodegradation. *Chem. Commun.* **2012**, *48*, 2858−2860.
(4) Lin, D.; Wu, H.; Zhang, R.; Pan, W. Enhanced Photocatalysis of Electrospun Ag−ZnO Heterostructured Nanofibers. *Chem. Mater.* **2009**, *21*, 3479−3484.
(5) Linic, S.; Christopher, P.; Ingram, D. B. Plasmonic-Metal Nanostructures for Efficient Conversion of Solar to Chemical Energy. *Nat. Mater.* **2011**, *10*, 911−921.
(6) Dong, Z.; Lai, X.; Halpert, J. E.; Yang, N.; Yi, L.; Zhai, J.; Wang, D.; Tang, Z.; Jiang, L. Accurate Control of Multishelled ZnO Hollow Microspheres for Dye-Sensitized Solar Cells with High Efficiency. *Adv. Mater.* **2012**, *24*, 1046−1049.
(7) Jiang, J.; Zhang, X.; Sun, P.; Zhang, L. ZnO/BiOI Heterostructures: Photoinduced Charge-Transfer Property and Enhanced Visible-Light Photocatalytic Activity. *J. Phys. Chem. C* **2011**, *115*, 20555−20564.
(8) Jeena, V.; Robinson, R. S. Convenient Photooxidation of Alcohols using Dye Sensitised Zinc Oxide in Combination with Silver Nitrate and TEMPO. *Chem. Commun.* **2012**, *48*, 299−301.
(9) Anandan, S.; Miyauchi, M. Ce-Doped ZnO (CexZn1-xO) Becomes an Efficient Visible-Light-Sensitive Photocatalyst by Co-Catalyst (Cu2+) Grafting. *Phys. Chem. Chem. Phys.* **2011**, *13*, 14937−14945.
(10) Fageria, P.; Gangopadhyay, S.; Pande, S. Synthesis of ZnO/Au and ZnO/Ag Nanoparticles and Their Photocatalytic Application using UV and Visible Light. *RSC Adv.* **2014**, *4*, 24962−24972.
(11) Georgekutty, R.; Seery, M. K.; Pillai, S. C. A Highly Efficient Ag-ZnO Photocatalyst: Synthesis, Properties, and Mechanism. *J. Phys. Chem. C* **2008**, *112*, 13563−13570.
(12) Han, Z.; Wei, L.; Zhang, Z.; Zhang, X.; Pan, H.; Chen, J. Visible-Light Photocatalytic Application of Hierarchical Au-ZnO Flower-Rod Heterostructures via Surface Plasmon Resonance. *Plasmonics* **2013**, *8*, 1193−1202.
(13) Clavero, C. Plasmon-Induced Hot-Electron Generation at Nanoparticle/Metal-Oxide Interfaces for Photovoltaic and Photocatalytic Devices. *Nat. Photonics* **2014**, *8*, 95−103.
(14) Mubeen, S.; Lee, J.; Singh, N.; Kramer, S.; Stucky, G. D.; Moskovits, M. An Autonomous Photosynthetic Device in which All Charge Carriers Derive From Surface Plasmons. *Nat. Nanotechnol.* **2013**, *8*, 247−251.
(15) Warren, S. C.; Thimsen, E. Plasmonic Solar Water Splitting. *Energy Environ. Sci.* **2012**, *5*, 5133−5146.
(16) Kochuveedu, S. T.; Kim, D.-P.; Kim, D. H. Surface-Plasmon-Induced Visible Light Photocatalytic Activity of TiO2 Nanospheres Decorated by Au Nanoparticles with Controlled Configuration. *J. Phys. Chem. C* **2012**, *116*, 2500−2506.
(17) Rong, G.; Wang, H.; Skewis, L. R.; Reinhard, B. M. Resolving Sub-Diffraction Limit Encounters in Nanoparticle Tracking Using Live Cell Plasmon Coupling Microscopy. *Nano Lett.* **2008**, *8*, 3386−3393.
(18) Feng, A. L.; You, M. L.; Tian, L.; Singamaneni, S.; Liu, M.; Duan, Z.; Lu, T. J.; Xu, F.; Lin, M. Distance-Dependent Plasmon-Enhanced Fluorescence of Upconversion Nanoparticles using Polyelectrolyte Multilayers as Tunable Spacers. *Sci. Rep.* **2015**, *5*, 7779.
(19) Wang, X.; He, F.; Zhu, X.; Tang, F.; Li, L. Hybrid Silver Nanoparticle/Conjugated Polyelectrolyte Nanocomposites Exhibiting Controllable Metal-Enhanced Fluorescence. *Sci. Rep.* **2014**, *4*, 4406.
(20) Cheng, H.; Huang, B.; Dai, Y. Engineering BiOX (X = Cl, Br, I) Nanostructures for Highly Efficient Photocatalytic Applications. *Nanoscale* **2014**, *6*, 2009−2026.
(21) Stuart, M. A. C.; Huck, W. T. S.; Genzer, J.; Muller, M.; Ober, C.; Stamm, M.; Sukhorukov, G. B.; Szleifer, I.; Tsukruk, V. V.; Urban, M.; Winnik, F.; Zauscher, S.; Luzinov, I.; Minko, S. Emerging Applications of Stimuli-Responsive Polymer Materials. *Nat. Mater.* **2010**, *9*, 101−113.
(22) Li, D.; Lee, J. Y.; Kim, D. H. Responsive Polymer/Gold Nanoparticle Composite Thin Films Fabricated by Solvent-Induced Self-Assembly and Spin-Coating. *J. Colloid Interface Sci.* **2011**, *354*, 585−591.
(23) Li, D.; Jang, Y. J.; Lee, J.; Lee, J.-E.; Kochuveedu, S. T.; Kim, D. H. Grafting Poly(4-vinylpyridine) onto Gold Nanorods toward Functional Plasmonic Core-Shell Nanostructures. *J. Mater. Chem.* **2011**, *21*, 16453−16460.
(24) Lee, J.-E.; Chung, K.; Jang, Y. H.; Jang, Y. J.; Kochuveedu, S. T.; Li, D.; Kim, D. H. Bimetallic Multifunctional Core@Shell Plasmonic Nanoparticles for Localized Surface Plasmon Resonance Based Sensing and Electrocatalysis. *Anal. Chem.* **2012**, *84*, 6494−6500.
(25) Ko, H.; Zhang, Z.; Chueh, Y.-L.; Saiz, E.; Javey, A. Thermoresponsive Chemical Connectors Based on Hybrid Nanowire Forests. *Angew. Chem., Int. Ed.* **2010**, *49*, 616−619.
(26) Zhang, R.; Mjoseng, H. K.; Hoeve, M. A.; Bauer, N. G.; Pells, S.; Besseling, R.; Velugotla, S.; Tourniaire, G.; Kishen, R. E. B.; Tsenkina, Y.; Armit, C.; Duffy, C. R. E.; Helfen, M.; Edenhofer, F.; de Sousa, P. A.; Bradley, M. A Thermoresponsive and Chemically Defined Hydrogel for Long-Term Culture of Human Embryonic Stem Cells. *Nat. Commun.* **2013**, *4*, 1335.
(27) Han, Y.; Nishimura, T.; Kato, T. Biomineralization-Inspired Approach to the Development of Hybrid Materials:Preparation of Patterned Polymer/Strontium Carbonate Thin Films Using Thermoresponsive Polymer Brush Matrices. *Polym. J.* **2014**, *46*, 499−504.
(28) Guan, Y.; Zhang, Y. PNIPAM Microgels for Biomedical Applications: from Dispersed Particles to 3D Assemblies. *Soft Matter* **2011**, *7*, 6375−6384.
(29) Mueller, M.; Tebbe, M.; Andreeva, D. V.; Karg, M.; Alvarez Puebla, R. A.; Pazos Perez, N.; Fery, A. Large-Area Organization of pNIPAM-Coated Nanostars as SERS Platforms for Polycyclic Aromatic Hydrocarbons Sensing in Gas Phase. *Langmuir* **2012**, *28*, 9168−9173.
(30) Contreras-Caceres, R.; Alonso-Cristobal, P.; Mendez-Gonzalez, D.; Laurenti, M.; Maldonado-Valdivia, A.; Garcia-Blanco, F.; López Cabarcos, E.; Fernandez-Barbero, A.; Lopez-Romero, J. M.; Rubio-Retama, J. Temperature Controlled Fluorescence on Au@Ag@PNIPAM-PTEBS Microgels: Effect of the Metal Core Size on the MEF Extension. *Langmuir* **2014**, *30*, 15560−15567.
(31) Tang, F.; Ma, N.; Tong, L.; He, F.; Li, L. Control of Metal-Enhanced Fluorescence with pH- and Thermoresponsive Hybrid Microgels. *Langmuir* **2012**, *28*, 883−888.
(32) Xue, C.; Yonet-Tanyeri, N.; Brouette, N.; Sferrazza, M.; Braun, P. V.; Leckband, D. E. Protein Adsorption on Poly(N-isopropylacrylamide) Brushes: Dependence on Grafting Density and Chain Collapse. *Langmuir* **2011**, *27*, 8810−8818.
(33) Zhao, W.; Krausch, G.; Rafailovich, M. H.; Sokolov, J. Lateral Structure of a Grafted Polymer Layer in a Poor Solvent. *Macromolecules* **1994**, *27*, 2933−2935.
(34) Plunkett, K. N.; Zhu, X.; Moore, J. S.; Leckband, D. E. PNIPAM Chain Collapse Depends on the Molecular Weight and Grafting Density. *Langmuir* **2006**, *22*, 4259−4266.
(35) Álvarez-Puebla, R. A.; Contreras-Cáceres, R.; Pastoriza-Santos, I.; Pérez-Juste, J.; Liz-Marzán, L. M. Au@pNIPAM Colloids as Molecular Traps for Surface-Enhanced, Spectroscopic, Ultra-Sensitive Analysis. *Angew. Chem., Int. Ed.* **2009**, *48*, 138−143.
(36) Contreras-Cáceres, R.; Pacifico, J.; Pastoriza-Santos, I.; Pérez-Juste, J.; Fernández-Barbero, A.; Liz-Marzán, L. M. Au@pNIPAM Thermosensitive Nanostructures: Control over Shell Cross-linking, Overall Dimensions, and Core Growth. *Adv. Funct. Mater.* **2009**, *19*, 3070−3076.
(37) Kumar, M. K.; Krishnamoorthy, S.; Tan, L. K.; Chiam, S. Y.; Tripathy, S.; Gao, H. Field Effects in Plasmonic Photocatalyst by Precise SiO2 Thickness Control Using Atomic Layer Deposition. *ACS Catal.* **2011**, *1*, 300−308.
(38) Awazu, K.; Fujimaki, M.; Rockstuhl, C.; Tominaga, J.; Murakami, H.; Ohki, Y.; Yoshida, N.; Watanabe, T. A Plasmonic Photocatalyst Consisting of Silver Nanoparticles Embedded in Titanium Dioxide. *J. Am. Chem. Soc.* **2008**, *130*, 1676−1680.

DOI: 10.1021/acsami.5b03872
ACS Appl. Mater. Interfaces 2015, 7, 21073−21081

(39) Zhang, X.; Zhu, Y.; Yang, X.; Wang, S.; Shen, J.; Lin, B.; Li, C. Enhanced Visible Light Photocatalytic Activity of Interlayer-Isolated Triplex Ag@SiO2@TiO2 Core-Shell Nanoparticles. *Nanoscale* **2013**, *5*, 3359−3366.
(40) Liu, Y.; Klep, V.; Zdyrko, B.; Luzinov, I. Synthesis of High-Density Grafted Polymer Layers with Thickness and Grafting Density Gradients. *Langmuir* **2005**, *21*, 11806−11813.
(41) Kasuya, M.; Taniguchi, T.; Motokawa, R.; Kohri, M.; Kishikawa, K.; Nakahira, T. Quantification of ATRP Initiator Density on Polymer Latex Particles by Fluorescence Labeling Technique using Copper-Catalyzed Azide-Alkyne Cycloaddition. *J. Polym. Sci., Part A: Polym. Chem.* **2013**, *51*, 4042−4051.
(42) Liu, Y.; Klep, V.; Zdyrko, B.; Luzinov, I. Polymer Grafting via ATRP Initiated from Macroinitiator Synthesized on Surface. *Langmuir* **2004**, *20*, 6710−6718.
(43) Matyjaszewski, K. Atom Transfer Radical Polymerization (ATRP): Current Status and Future Perspectives. *Macromolecules* **2012**, *45*, 4015−4039.
(44) Zhang, G.; Shen, X.; Yang, Y. Facile Synthesis of Monodisperse Porous ZnO Spheres by a Soluble Starch-Assisted Method and Their Photocatalytic Activity. *J. Phys. Chem. C* **2011**, *115*, 7145−7152.
(45) Takahata, R.; Yamazoe, S.; Koyasu, K.; Tsukuda, T. Surface Plasmon Resonance in Gold Ultrathin Nanorods and Nanowires. *J. Am. Chem. Soc.* **2014**, *136*, 8489−8491.
(46) Yu, Z. B.; Xie, Y. P.; Liu, G.; Lu, G. Q.; Ma, X. L.; Cheng, H.-M. Self-assembled CdS/Au/ZnO heterostructure induced by surface polar charges for efficient photocatalytic hydrogen evolution. *J. Mater. Chem. A* **2013**, *1*, 2773−2776.
(47) Wang, Z.; Yang, C.; Lin, T.; Yin, H.; Chen, P.; Wan, D.; Xu, F.; Huang, F.; Lin, J.; Xie, X.; Jiang, M. H-Doped Black Titania with Very High Solar Absorption and Excellent Photocatalysis Enhanced by Localized Surface Plasmon Resonance. *Adv. Funct. Mater.* **2013**, *23*, 5444−5450.
(48) Weickert, J.; Palumbiny, C.; Nedelcu, M.; Bein, T.; Schmidt-Mende, L. Controlled Growth of TiO2 Nanotubes on Conducting Glass. *Chem. Mater.* **2011**, *23*, 155−162.
(49) Augugliaro, V.; Palmisano, L.; Sclafani, A.; Minero, C.; Pelizzetti, E. Photocatalytic Degradation of Phenol in Aqueous Titanium Dioxide Dispersions. *Toxicol. Environ. Chem.* **1988**, *16*, 89−109.
(50) Pincella, F.; Isozaki, K.; Miki, K. A Visible Light-Driven Plasmonic Photocatalyst. *Light: Sci. Appl.* **2014**, *3*, e133.
(51) Dao, T. D.; Han, G.; Arai, N.; Nabatame, T.; Wada, Y.; Hoang, C. V.; Aono, M.; Nagao, T. Plasmon-mediated photocatalytic activity of wet-chemically prepared ZnO nanowire arrays. *Phys. Chem. Chem. Phys.* **2015**, *17*, 7395−7403.
(52) Bumajdad, A.; Madkour, M. Understanding the superior photocatalytic activity of noble metals modified titania under UV and visible light irradiation. *Phys. Chem. Chem. Phys.* **2014**, *16*, 7146−7158.
(53) Welford, K. Surface plasmon-polaritons and their uses. *Opt. Quantum Electron.* **1991**, *23*, 1−27.
(54) Pelayo Garcia de Arquer, F.; Mihi, A.; Konstantatos, G. Molecular interfaces for plasmonic hot electron photovoltaics. *Nanoscale* **2015**, *7*, 2281−2288.
(55) Wang, J.-g.; Pan, X.; Zhuang, G.-l.; Lu, X.-h. Computational Catalysis in Nanotubes. In *Catalysis*, Vol. *26*; The Royal Society of Chemistry: London, 2014; Chapter 4, pp 109−160.
(56) Rajbongshi, B. M.; Ramchiary, A.; Jha, B. M.; Samdarshi, S. K. Synthesis and Characterization of Plasmonic Visible Active Ag/ZnO Photocatalyst. *J. Mater. Sci.: Mater. Electron.* **2014**, *25*, 2969−2973.

DOI: 10.1021/acsami.5b03872
ACS Appl. Mater. Interfaces 2015, 7, 21073−21081